Macromolecules

Article

pubs.acs.org/Macromolecules

Structural Diversity and Phase Behavior of Brush Block Copolymer Nanocomposites

Dong-Po Song, Yue Gai, Benjamin M. Yavitt, Alexander Ribbe, Samuel Gido, and James J. Watkins*

Department of Polymer Science and Engineering, University of Massachusetts Amherst, 120 Governors Drive, Amherst, Massachusetts 01003, United States

Supporting Information

ABSTRACT: Brush block copolymers (BBCPs) exhibit attractive features for use as templates for functional hybrid nanomaterials including rapid ordering dynamics and access to broad ranges of domain sizes; however, there are relatively few studies of the morphology of the BBCPs as a function of their structural variables and fewer still studies of BBCP composite systems. Here we report the structural diversity and phase behavior of one class of BBCP nanocomposites as a function of the volume fractions of their components and the side chain symmetry of the BBCPs. We conducted a systematic investigation of gold nanoparticle (NP) (~2 nm) assembly in a series of poly(*tert*-butyl acrylate)-*block*-poly(ethylene oxide) (P*t*BA-*b*-PEO) BBCPs with a fixed side chain length of P*t*BA (M_n = 8.2 kg/mol) but with different PEO brush lengths (M_n = 5.0, 2.0, or 0.75 kg/mol) as well as volume fractions (f_{PEO} = 0.200−0.484). The gold NPs are selectively incorporated within the PEO domain via hydrogen bond interactions between the 4-mercaptophenol ligands of the gold NPs and the PEO side chains. A number of morphological transitions were observed and were dependent on the total volume fraction ($f_{NP/PEO}$) of NPs and PEO domain. Symmetric or asymmetric lamellar morphologies of NP arrays were readily created through simple variation of $f_{NP/PEO}$. Interestingly, a lamellar structure was obtained at a small $f_{NP/PEO}$ of only 0.248 for nanocomposites based on BBCPs with comparable side chain lengths (MW_{PEO}/MW_{PtBA} = 0.63). In contrast, NP morphological transitions from wormlike through cylindrical to lamellar structures were observed with the increase of $f_{NP/PEO}$ for nanocomposites based on BBCPs with a large difference in side chain length (MW_{PEO}/MW_{PtBA} = 0.09). Highly deformed cylinders were observed in the cylindrical morphology as clearly identified by high angle annular dark field (HAADF) scanning transmission electron microscopy (STEM) tomography. This work represents a starting point for understanding BBCP composite phase behavior, and it provides new insight toward strategies for control over the microstructure of NP arrays assembled in BBCP templates, which is essential for functional materials design.

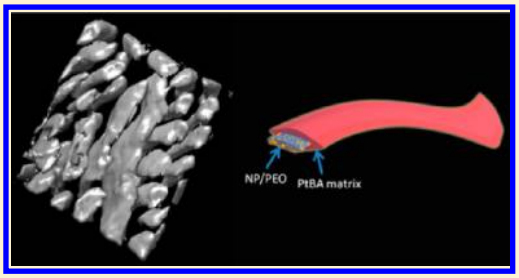

INTRODUCTION

Control over the spatial arrangements of functional nanoparticles (NPs) at the nanoscale level is central to the bottom-up manufacturing of next-generation materials for many important applications such as optical, electronic, and optoelectronic nanodevices.[1−7] Block copolymers (BCPs) have been widely used in the directed assembly of NPs via microphase separation, affording periodically nanostructured hybrid materials with a combination of the processability and mechanical properties of polymers with the attractive physical properties of NP arrays.[8−10]

Over the past two decades, most of the studies regarding BCP/NP hybrids have focused on the assembly of NPs using linear BCPs (LBCPs).[11−24] A balance between enthalpic contribution due to BCP/NP interactions and entropic penalty arising from polymer chain stretching for NP incorporation is generally considered as the key factor that determines the dispersion of NPs.[14] Favorable interactions between NPs and specific domains of LBCPs have been typically required to achieve selective incorporation and good dispersion of NPs within the target domains of the resulting nanocomposites. Neutral or weak BCP/NP interactions, such as van der Waals interaction, lead to limited loading of NPs in nanocomposites,[8−17] while strong interactions, such as hydrogen bonding and ionic interactions, significantly increase NP loading.[18−22] In addition, small molecules were also employed as the intermediate agents between BCPs and NPs to enhance the stability of the resulting nanocomposites.[23,24] Macrophase aggregation of NPs is often observed when the NP loading increases to a high level due to large entropy loss and NP jamming effect.[21,24] Moreover, there are several other limitations for LBCPs that greatly affect the utility of BCP/NP hybrids, including the slow ordering kinetics, small domain sizes, limited NP sizes, and poor long-range order.

Brush BCPs (BBCPs) represent a major step forward in BCP-based materials relative to traditional LBCPs. Well-ordered nanostructures are able to be created in a few minutes benefiting from substantially reduced polymer chain entangle-

Received: July 24, 2016
Revised: August 26, 2016

DOI: 10.1021/acs.macromol.6b01602
Macromolecules XXXX, XXX, XXX−XXX

ments relative to their linear analogues.[25−34] Recently, we have reported several initial studies of NP assembly in BBCPs.[35−38] In comparison to LBCPs, BBCPs exhibit many advantages for the directed assembly of NPs, including well-ordered structures developed under high NP loading, rapid ordering kinetics on the order of a few minutes, large domain spacing over 100 nm, enhanced capability for incorporating NPs larger than 10 nm,[35] and the observation of long-range order over large volume elements.[37] However, the structural diversity and phase behavior of BBCP/NP composites in terms of volume fraction and side chain symmetry of BBCPs remain unclear. A thorough understanding of the phase behavior will enable full exploration of the tool box of BBCPs for NP assembly but also provide the framework for future systematic studies on structure−function relationships in architected periodic hybrid materials.

We present a systematic investigation of NP assembly in a series of poly(*tert*-butyl acrylate)-*block*-poly(ethylene oxide) (P*t*BA$_n$-*b*-PEO$_m$) BBCPs with a fixed side chain length of P*t*BA (n = 8.2K; M_n = 8.2 kg/mol) but different PEO brushes with precisely controlled molecular weights (MWs) (m = 5.0K, 2.0K, and 0.75K; M_n = 5.0, 2.0, or 0.75 kg/mol) and volume fractions (f_{PEO} = 0.200−0.484). Here, the side chain asymmetry expresses as a ratio of MWs (MW_{PEO}/MW_{PtBA}). A smaller value indicates more asymmetry in side chain length of the BBCP. Small gold NPs (∼2 nm) coated with 4-mercaptophenol are chosen as the model system for the investigation. The NPs are selectively incorporated within the PEO domain through hydrogen bonding between NP ligands and PEO block. Briefly, there are three different groups of samples based on side chain variation, and each exhibits interesting behavior as summarized below as subsequently discussed in detail:

Group I (P*t*BA$_{8.2K}$-*b*-PEO$_{5.0K}$). For relatively symmetric BBCPs (MW_{PEO}/MW_{PtBA} = 0.63), lamellar morphologies were obtained in a wide range of the total volume fraction of NPs and PEO ($f_{NP/PEO}$) from approximately 0.248 to 0.634.[37] For comparison, the lamellar window is typically between 0.400 and 0.650 in LBCP/NP composite systems.[18,21] Moreover, it was observed for the first time that a morphological transition from lamellae to inverse cylinder was induced by increasing $f_{NP/PEO}$ in BBCP-based nanocomposites.

Group II (P*t*BA$_{8.2K}$-*b*-PEO$_{2.0K}$). By decreasing the side chain symmetry (MW_{PEO}/MW_{PtBA} = 0.24), wormlike morphologies were obtained in the nanocomposites at $f_{NP/PEO}$ ranging from 0.237 to 0.433. Interestingly, a phase transition from wormlike into a lamellar morphology occurred with a further increase of $f_{NP/PEO}$ to 0.512.

Group III (P*t*BA$_{8.2K}$-*b*-PEO$_{0.75K}$). For the significantly asymmetric BBCPs (MW_{PEO}/MW_{PtBA} = 0.09), NP morphological transitions from wormlike through cylindrical to lamellar structures were observed that were dependent on $f_{NP/PEO}$. Highly deformed cylinders were observed in the cylindrical morphology as clearly identified by high angle annular dark field (HAADF) scanning transmission electron microscopy (STEM) tomography.

EXPERIMENTAL SECTION

General Methods. Small-angle X-ray scattering (SAXS) measurements were performed with a Ganesha SAXS-LAB using 0.154 nm (Cu K radiation), sample-to-detector distance was 1491 mm, and X-ray beam area was 0.04 mm^2. Ultrasmall-angle X-ray scattering (USAXS) measurements were performed using a Xeuss USAXS equipment at the Changchun Institute of Applied Chemistry (CIAC) in China. The wavelength of X-ray was 0.154 nm, beam area was 0.6 × 0.6 mm^2, and sample-to-detector distance was 6558 mm. Transmission electron microscopy (TEM) measurements were conducted with a JEOL 2000FX TEM operated at an accelerating voltage of 200 kV. Composite samples were embedded in epoxy and cured at room temperature overnight. Thin sections of approximately 50 nm in thickness for microscopy were prepared using a Leica Ultracut UCT microtome equipped with a Leica EM FCS cryogenic sample chamber operated at −80 °C. Scanning transmission electron microscopy in high angle annular dark field imaging mode (STEM-HAADF) tomography was carried out using a JEOL JEM-2200FS at 200 kV acceleration voltage and a probe size of 1.5 nm. Image series of 121 images for tomography reconstruction were recorded at 1° steps from −60° to +60° tilt angles. Three-dimensional reconstructions were generated using the filtered back projection algorithm in Etomo (part of the IMOD software package, UC Boulder). Volume and isosurface rendering were performed using Chimera (UCSF). ^{1}H NMR spectroscopy was recorded in $CDCl_3$ using a Bruker Avance DPX 500 NMR spectrometer. Gel permeation chromatography (GPC) of the bottle brush copolymers was carried out in THF on two PLgel 10 μm mixed-B LS columns (Polymer Laboratories) connected in series with a DAWN EOS multiangle laser light scattering (MALLS) detector and an RI detector. No calibration standards were used for the bottle brush copolymers, and dn/dc values were obtained for each injection by assuming 100% mass elution from the columns.

Sample Preparation. Stainless steel washers together with Kapton film were used as the molds for sample preparations. The inside diameter and the thickness of the washer are 5.0 and 1.0 mm, respectively. Neat polymer samples were made by filling polymer solid into the washer following by thermal annealing at 110 °C for about 5 min. In some cases, a cross-linked flat PDMS pad was used to gently press the samples in the vertical direction to make the top surface flat. For BCP-NP composite samples, appropriate amounts of BBCPs were weighed and dissolved in anhydrous tetrahydrofuran (THF) followed by adding NP solutions in the same solvent to form about 2% (w/v) stock solutions. The THF solutions were cast through 0.4 μm PTFE filters onto horizontal glass substrates which were covered immediately with glass Petri dishes. The evaporation process was carried out for at least 5 h, during which phase segergation and self-assembly occurred. After solvent evaporation, the dried films were removed from glass using a razor blade and filled in a washer at 110 °C. The resulting bulk samples were subsequently kept at 110 °C for about 5 min, sealed using Kapton films, and then cooled to room temperature in air before SAXS measurement. We note that the evaporation of THF solutions was carried out under a nitrogen atmosphere to control humidity below 20%.

RESULTS AND DISCUSSION

The BBCPs used in this work are well-defined (polynorbornene-*graft*-poly(*tert*-butyl acrylate))-*block*-(polynorbornene-*graft*-poly(ethylene oxide)) BBCPs synthesized by sequential ring-opening metathesis polymerization (ROMP). Detailed information regarding the synthesis and characterizations of the polymers has been reported previously or shown in the Supporting Information (Figures S1 and S2).[37,38] The molecular weight information for the P*t*BA-*b*-PEO BBCPs is summarized in Table 1. The grafting-through method not only enables precise control over the MW of side chain but also ensures a 100% grafting density of the BBCPs. The BBCP/NP nanocomposites were prepared through evaporation of the mixture solutions with anhydrous tetrahydrofuran (THF) as the solvent (see Experimental Section for details). Herein the volume fraction (f_{NP}) of NPs (core + ligand) can be estimated using the densities of the components (see Supporting Information).

Group I: Nanocomposites of P*t*BA$_{8.2K}$-*b*-PEO$_{5.0K}$ (MW_{PEO}/MW_{PtBA} = 0.63). We first investigate the phase behavior of BBCP/NP nanocomposites based on BBCPs with

DOI: 10.1021/acs.macromol.6b01602
Macromolecules XXXX, XXX, XXX−XXX

Table 1. Molecular Weight Information for the (Polynorbornene-*graft*-Poly(*tert*-butyl acrylate))-*block*-(Polynorbornene-*graft*-Poly(ethylene oxide)) Copolymers

BBCP	M_n[a] (kg/mol)	PDI[a]	DP[b] PSMM	DP[b] PEOMM	f_{PEO}[c]
group I ($PtBA_{8.2K}$-*b*-$PEO_{5.0K}$)					
A	504.9	1.15	48	21	0.212
B	1590	1.15	128	108	0.323
C	2694	1.08	261	169	0.484
D	1850	1.12	179	116	0.484
group II ($PtBA_{8.2K}$-*b*-$PEO_{2.0K}$)					
E	1810	1.31	177	181	0.200
F	347.9	1.27	23	80	0.462
group III ($PtBA_{8.2K}$-*b*-$PEO_{0.75K}$)					
G	361.5	1.25	32	134	0.278
H	1130	1.12	72	714	0.474

[a]Molecular weight and polydispersity index as measured by GPC-MALLS. [b]Approximation of the size of each block as calculated using NMR and GPC results. [c]The volume fraction of PEO block (f_{PEO}) as determined by NMR data.

relatively symmetric side chains. Figure 1a shows one-dimensional small-angle X-ray scattering (1D SAXS) results for BBCP-**A** (f_{PEO} = 0.212) and blends of the polymer with different volume fractions of NPs (f_{NP}) corresponding to different volume fractions of the NPs and PEO domain ($f_{NP/PEO}$). A sharp primary peak (q) was observed in 1D SAXS patterns of the neat polymer, which is indicative of a strong microphase separation. However, no higher order reflections can be indentified due to a poor long-range order (Figure 1a). A higher order peak located at 2q was observed upon adding a small amount of NPs (f_{NP} = 0.046), suggesting the probable formation of a lamellar morphology at an exceptionally small $f_{NP/PEO}$ of 0.248. The asymmetric lamellar morphology was further confirmed by higher order peaks at 4q for nanocomposites with higher f_{NP} (0.105 and 0.155) as indicated by Figure 1a, corresponding to higher $f_{NP/PEO}$ (0.295 and 0.334). The highly asymmetric lamellar morphology can be attributed to the rigid molecular backbone of the BBCP which favors flat domain interfaces of lamellar structures even for samples with highly asymmetric volume fractions.[39−41] For comparison, lamellar morphologies have been typically obtained at volume fractions of the NP incorporated domain between 0.480 and 0.650 for LBCP/NP composites.[21] Figure 2a shows TEM micrographs of microtomed samples. For the neat polymer (BBCP-**A**), a poorly ordered state is shown in the TEM ($f_{NP/PEO}$ = 0.212) consistent with the SAXS result (Figure 1a). For composite samples, we note that since P*t*BA and PEO domains of the unstained composite samples have similar electron densities, the contrast observed in the TEM images is evidently due to the gold NPs residing exclusively in PEO domains. As shown in Figure 2a, asymmetric lamellar morphologies are confirmed in nanocomposites with small $f_{NP/PEO}$ (0.248 and 0.334). Wormlike morphologies can also be seen in the TEM micrographs, suggesting the influence of morphology by volume fraction may be non-negligible (see discussions below). Further increasing NP loading results in more symmetric lamellar structures as indicated by the appearance of higher order peaks at 3q in SAXS (Figure 1a) at higher $f_{NP/PEO}$ (0.382 and 0.442). The multiple higher order peaks in 1D SAXS (Figure 1a) are missing with a further increased f_{NP} to 0.390 ($f_{NP/PEO}$ = 0.519) corresponding to an ultrahigh volume fraction (0.751) of NPs in the PEO domain. Despite the losing of long-range order, strong phase separation of the highly loaded sample was maintained as indicated by the strong primary peak in the 1D SAXS results ($f_{NP/PEO}$ = 0.519). The domain spacing gradually increased from 51 to 68 nm with the increased f_{NP} from 0 to 0.390, or $f_{NP/PEO}$ from 0.212 to 0.519, due to the swelling of PEO domain by the NPs incorporated.

Figure 1b shows the 1D SAXS of composite samples using BBCP-**B** (f_{PEO} = 0.323). A morphological transition from disordered cylinder to a lamellar structure was observed at $f_{NP/PEO}$ values of up to 0.394 (f_{NP} = 0.105) as confirmed by the higher order peak at 3q. Symmetric lamellar morphologies were obtained in nanocomposites with $f_{NP/PEO}$ increasing from 0.469 to 0.520 (f_{NP} from 0.215 to 0.291) as indicated by the higher order reflections at 3q and 5q in SAXS (Figure 1b). The morphological transition and the symmetric lamellar structure were further confirmed by TEM in Figure 2b. Morover, inverse asymmetric lamellar structures were developed in the composite samples containing BBCP-**D** (f_{PEO} = 0.484) and

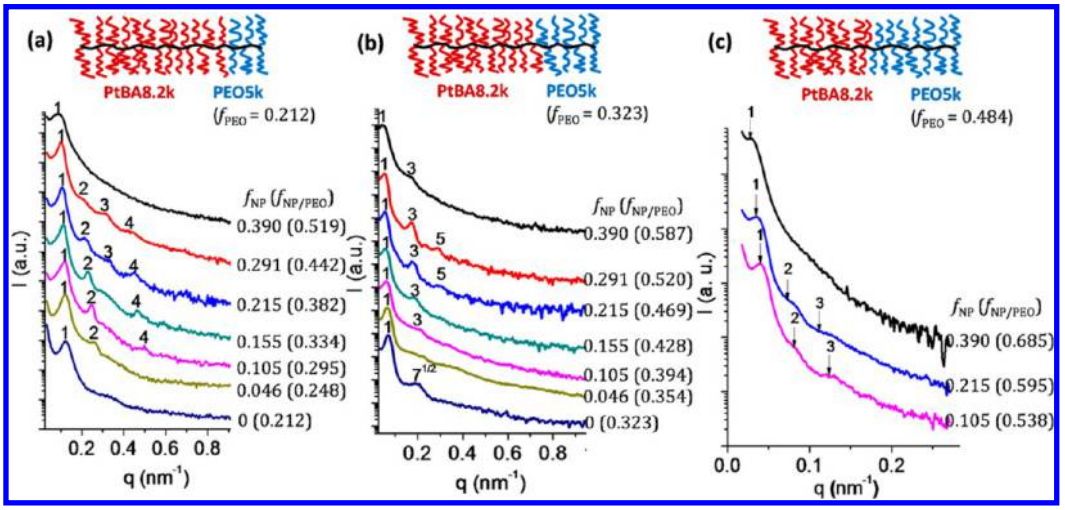

Figure 1. (a, b) 1D SAXS profiles of blends of BBCP-**A** (f_{PEO} = 0.212) and BBCP-**B** (f_{PEO} = 0.323) with gold NPs at different volume fractions of NPs (f_{NP}), showing asymmetric and symmetric lamellar morphologies formed that are dependent on total volume fraction ($f_{NP/PEO}$) of the NP incorporated PEO domain. (c) 1D USAXS profiles of blends of BBCP-**C** (f_{PEO} = 0.484) with the indicated f_{NP} and $f_{NP/PEO}$.

DOI: 10.1021/acs.macromol.6b01602
Macromolecules XXXX, XXX, XXX−XXX

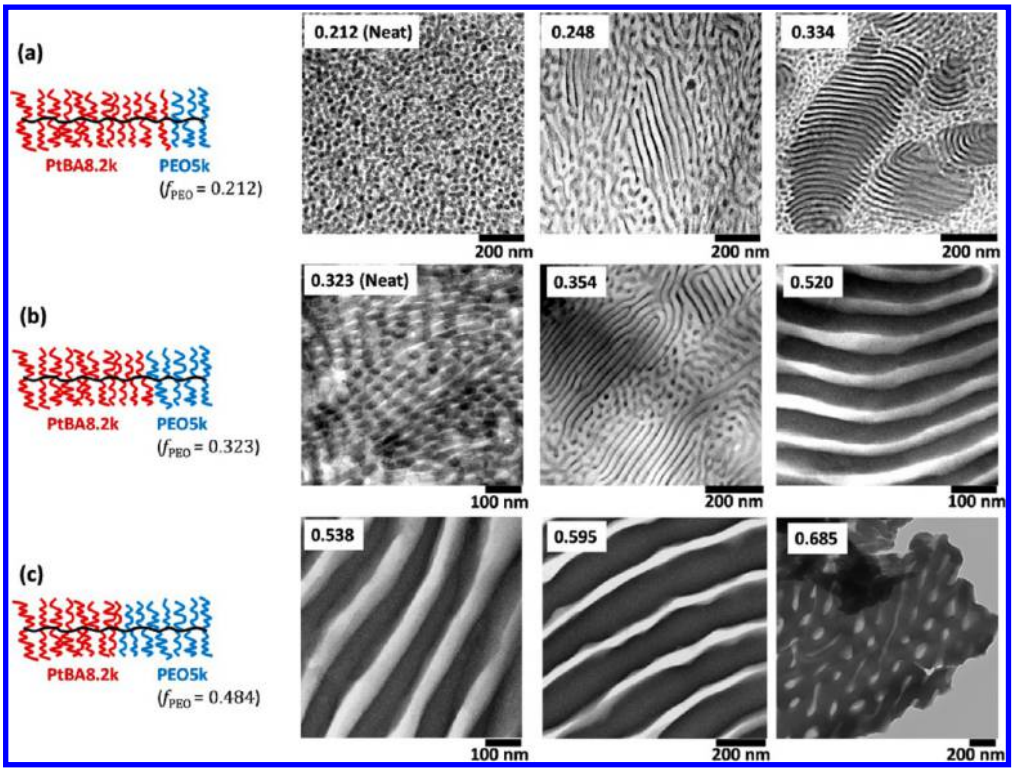

Figure 2. Cross-sectional TEM micrographs of blends of (a) BBCP-**A**, (b) -**B**, and (c) -**C** with gold NPs at the indicated volume fractions. The inset numbers refer to the total volume fractions ($f_{NP/PEO}$) of the NP incorporated PEO domain. Neat polymers (left-hand column) were stained with RuO_4 vapor, resulting in PEO domain appearing as the dark regions. No staining was applied to the composite samples.

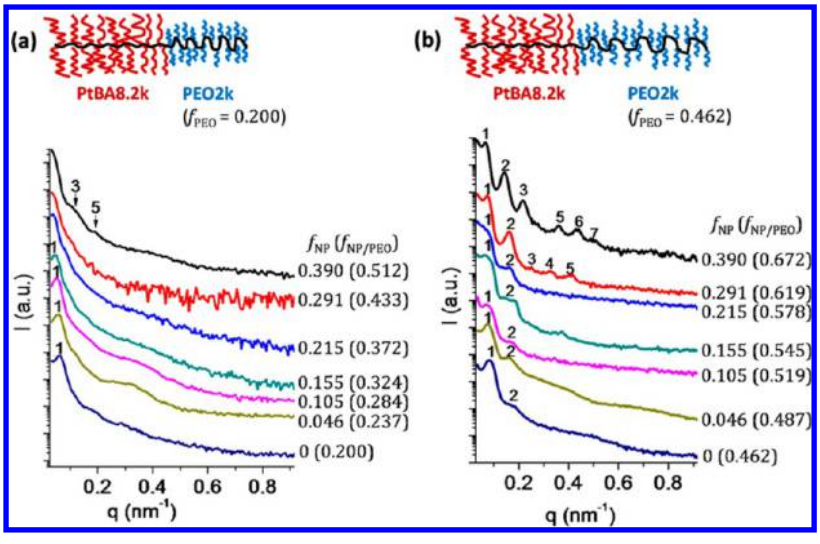

Figure 3. 1D SAXS profiles of blends of (a) BBCP-**E** (f_{PEO} = 0.200) and (b) BBCP-**F** (f_{PEO} = 0.462) with gold NPs at the indicated loading volume fractions, showing morphological transitions that are dependent on volume fractions ($f_{NP/PEO}$) of the NP incorporated PEO domains.

gold NPs at a f_{NP} value over 0.215 ($f_{NP/PEO}$ = 0.595) (see our previous publication for details).[37] In addition, Figure 1c shows one-dimensional ultrasmall-angle X-ray scattering (1D USAXS) profiles of blends of BBCP-**C** (f_{PEO} = 0.484) with different loadings of NPs. Lamellar morphologies were verified at $f_{NP/PEO}$ values of 0.538 and 0.595 (f_{NP} = 0.105 and 0.215) by the presence of multiple order peaks at 1q, 2q, and 3q in USAXS (Figure 1c). The well-ordered lamellar morphologies of the NP arrays were further confirmed by TEM in Figure 2c. Interestingly, a morphological transition from lamellae to inverse cylinder or wormlike structures was observed at a high $f_{NP/PEO}$ (0.685) as indicated by both USAXS and TEM (Figures 1c and 2c). The domain spacing increases from 157 to 224 nm with the increased f_{NP} from 0.215 to 0.390 corresponding to $f_{NP/PEO}$ from 0.595 to 0.685 (Figure 1c). The lamellar nanocomposites of large lattice spacing can reflect visible light, and the reflection maximum increases with the increase of lattice spacing.[36,38] Here, an abnormal blue-shift of the reflection maximum as well as a broadened reflection peak was observed with an increase of the f_{NP} from 0.215 to 0.390 ($f_{NP/PEO}$ from 0.595 to 0.685) (Figure S3) due to the morphology-transition-induced vibrations in lattice parameters

DOI: 10.1021/acs.macromol.6b01602
Macromolecules XXXX, XXX, XXX−XXX

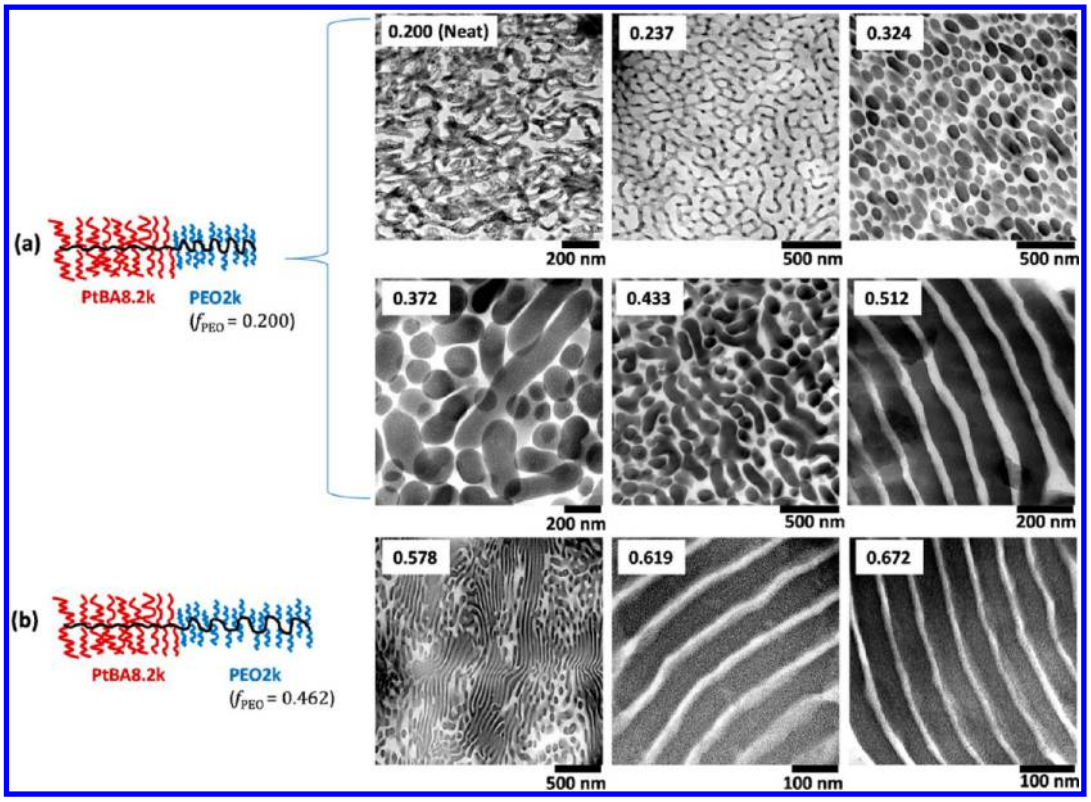

Figure 4. Cross-sectional TEM micrographs of blends of (a) BBCP-**E** (f_{PEO} = 0.200) and (b) BBCP-**F** (f_{PEO} = 0.462) with gold NPs at the indicated loading volume fractions. The inset numbers refer to volume fractions ($f_{NP/PEO}$) of the NP incorporated PEO domain. Neat polymers (left-hand column) were stained with RuO_4 vapor with PEO domain appearing as the dark regions. No staining was applied on composite samples.

of the photonic crystal structure.[36,38] To our knowledge, it is for the first time that a morphology transition was achieved by increasing the volume fraction of the NP domain in BBCP composite systems. This is different from our previous observation of a phase transition induced by variations in side chain symmetry through the addition of large NPs into BBCPs.[35]

Group II: Nanocomposites of P*t*BA$_{8.2K}$-*b*-PEO$_{2.0K}$ (MW$_{PEO}$/MW$_{PtBA}$ = 0.24). We next investigate the phase behavior of composites based on asymmetric BBCPs with the molecular weight of PEO brush much smaller than that of P*t*BA (MW$_{PEO}$/MW$_{PtBA}$ = 0.24). Figure 3a shows the 1D SAXS profiles of BBCP-**E** (f_{PEO} = 0.200) and a series of composite samples containing different concentrations of NPs. A gradual shift of the primary peak to smaller q regions was observed when increasing f_{NP} from 0 to 0.390 or $f_{NP/PEO}$ from 0.200 to 0.512. The domain spacing increased from 97 to 161 nm, suggesting the confinement of NPs exclusively within the PEO domain. Nevertheless, no higher order reflections can be verified in 1D SAXS of either the neat polymer or composite samples with f_{NP} ranging from 0.046 to 0.291, corresponding to $f_{NP/PEO}$ from 0.237 to 0.433 (Figure 3a). Interestingly, a morphological transition from the poorly ordered state to a well-ordered lamellar structure was verified at f_{NP} of 0.390 ($f_{NP/PEO}$ = 0.512) as confirmed by the appearance of higher ordered peaks at 3q and 5q in SAXS (Figure 3a). The morphological evolution was further confirmed by TEM. As shown in Figure 4a, a wormlike structure was observed in the neat polymer ($f_{NP/PEO}$ = 0.200) consistent the SAXS result (Figure 3a). For the composite samples, an interesting network structure of NP worms was formed at f_{NP} ~ 0.046 ($f_{NP/PEO}$ = 0.237). Further increasing NP loading lead to mixed morphologies with both wormlike and spherical features as evident in TEM micrographs at $f_{NP/PEO}$ ranging from 0.324 to 0.433 (see Figure 4a). This is generally different from the lamellar morphologies obtained in nanocomposites based on symmetric BBCP-**A** (see Figure 1a), suggesting that the decrease in side chain symmetry can generate a significantly affect the molecular chain packing of the supramolecular composites. Surprisingly, a morphological transition from the wormlike into a symmetric lamellar structure occurred at f_{NP} ~ 0.390 ($f_{NP/PEO}$ = 0.512) consistent with the SAXS results (Figure 3a vs 4a). All the results indicate that volume fraction of the NP incorporated PEO domain ($f_{NP/PEO}$) is a very important factor that can greatly influence the morphology of nanocomposites based on BBCPs with asymmetric side chain lengths.

Figure 3b shows the 1D SAXS data of a series of composite samples based on BBCP-**F** (f_{PEO} = 0.462). A lamellar morphology was formed in the neat polymer sample as indicated by the X-ray scattering peaks at 1q and 2q. Similar lamellar morphologies were also observed in the composite samples at f_{NP} from 0.046 to 0.215, corresponding to $f_{NP/PEO}$ from 0.487 to 0.578 (see Figure 3b and TEM 0.578 in Figure 4b). The lamellar structure was greatly improved in terms of long-range order at an increased f_{NP} of 0.291 ($f_{NP/PEO}$ = 0.619) as indicated by the multiple higher order peaks at 2q, 3q, 4q, and 5q (see Figure 3b). The improvement of ordering was further confirmed by TEM shown in Figure 4b (see TEM 0.619). The highly ordered lamellar structure of NP arrays was maintained at a higher NP concentration (f_{NP} = 0.390, $f_{NP/PEO}$ = 0.672) as confirmed by both SAXS and TEM results (Figures 3b and 4b). Briefly, the lamellar morphology was developed with $f_{NP/PEO}$ ranging from 0.487 to 0.672, which is close to the

DOI: 10.1021/acs.macromol.6b01602
Macromolecules XXXX, XXX, XXX−XXX

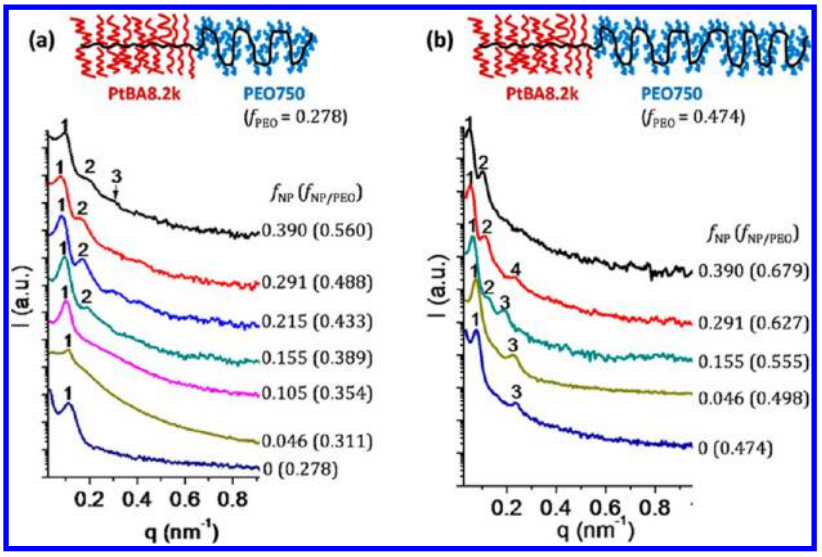

Figure 5. 1D SAXS profiles of blends of (a) BBCP-**G** (f_{PEO} = 0.278) and (b) BBCP-**H** (f_{PEO} = 0.474) with gold NPs at different volume fractions, showing morphological transitions dependent on volume fractions ($f_{NP/PEO}$) of the NP incorporated PEO domain.

lamellar window (0.480−0.650) for nanocomposites based on LBCP systems such as poly(styrene-*block*-2-vinylpyrindine) (PS-*b*-P2VP).[21]

Group III: Nanocomposites of P*t*BA$_{8.2K}$-*b*-PEO$_{0.75K}$ (MW$_{PEO}$/MW$_{PtBA}$ = 0.09). We further study the phase behavior of BBCP/NP nanocomposites using extremely asymmetric P*t*BA-*b*-PEO BBCPs. The MW of the PEO side chain is only 0.75 kg/mol, which is about 9% of the MW of P*t*BA side chain (8.2 kg/mol). As a result, the molecular backbone of the PEO block is expected to be much more flexible relative to the P*t*BA block. Figure 5a shows the 1D SAXS of the neat polymer sample as well as composite samples based on BBCP-**G** (f_{PEO} = 0.278). As shown in the figure, the neat polymer exhibited strong phase segregation but was relatively disordered as indicated by the only sharp primary order peak observed in SAXS. Similar morphologies were also observed in the composite samples at f_{NP} of 0.046 and 0.105, corresponding to $f_{NP/PEO}$ of 0.311 and 0.354 (see Figure 5a). A TEM micrograph ($f_{NP/PEO}$ = 0.311) in Figure 6 indicates a randomly distributed wormlike structure, consistent with the SAXS data (Figure 5a). Interestingly, higher order scattering peaks located at 2q are observed in SAXS at $f_{NP/PEO}$ ranging from 0.389 to 0.488, indicating a relatively ordered state in the structure. A cylindrical morphology was shown in TEM micrographs of the samples (see TEM 0.389 and 0.433 in Figure 6). Moreover, the cylinder morphology was also confirmed by a good fitting of the form factor peaks observed in SAXS ($f_{NP/PEO}$ = 0.433) using a cylinder model (see Figure S4).

The interesting structures were further characterized by scanning TEM (STEM) using a high-angle annular dark-field (HAADF) detector. As shown in Figures 7a and 7b, the bright regions are gold NPs selectively sequestered within the PEO domain. Highly deformed cylinders with a relative constant spacing were observed in Figure 7a. HAADF-STEM tomography was employed to further characterize the morphology. Impressively, highly distorted cylinders, some NP belt-like features, were clearly shown in the reconstructed three-dimensional (3D) structures at different viewing angles (Figure 7c−e). The NP incorporated PEO domain is embedded in the P*t*BA matrix as indicated by Figure 7f. These cylinders of NPs (Figure 7e) have enough packing coherence to produce a

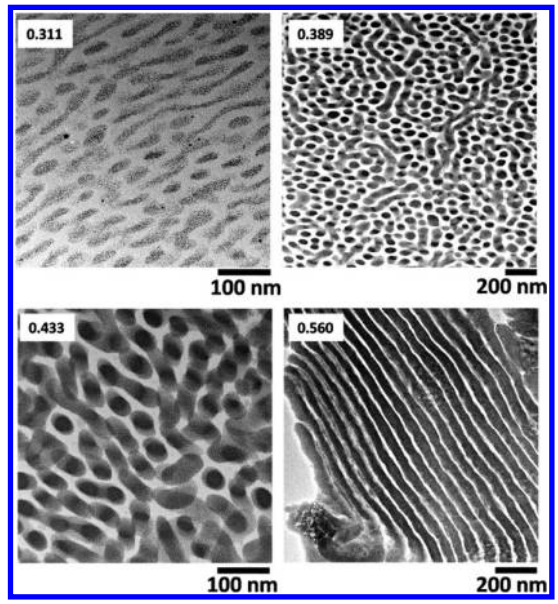

Figure 6. Cross-sectional TEM micrographs of blends of BBCP-**G** (f_{PEO} = 0.278) with gold NPs at different volume fractions. The inset numbers refer to volume fractions ($f_{NP/PEO}$) of the NP incorporated PEO domain. No staining was applied on composite samples.

strong second-order Bragg peak in SAXS ($f_{NP/PEO}$ = 0.433 in Figure 5a). The domain spacing is approximately 74 nm as calculated using the primary order peak located at q = 0.085. The highly distorted cylinders are likely a result of packing frustrations in a disordered arrangement of cylinders and may be enabled by both the Au NP incorporation and the asymmetric molecular structure of BBCP-**G** with a large difference in side chain lengths. Interestingly, further increasing the f_{NP} to 0.390 ($f_{NP/PEO}$ = 0.560) results in a morphological transition from the cylinders into a lamellar structure as indicated by SAXS in Figure 5a as well as the TEM micrograph (TEM 0.560) in Figure 6. The domain spacing increased from 57 to 82 nm with NP loading f_{NP} increased from 0 to 0.291 as indicated by SAXS shown in Figure 5a. However, a further increase of f_{NP} to 0.390 resulted in a decrease of domain spacing from 82 to 65 nm (Figure 5a). At this particular

DOI: 10.1021/acs.macromol.6b01602
Macromolecules XXXX, XXX, XXX−XXX

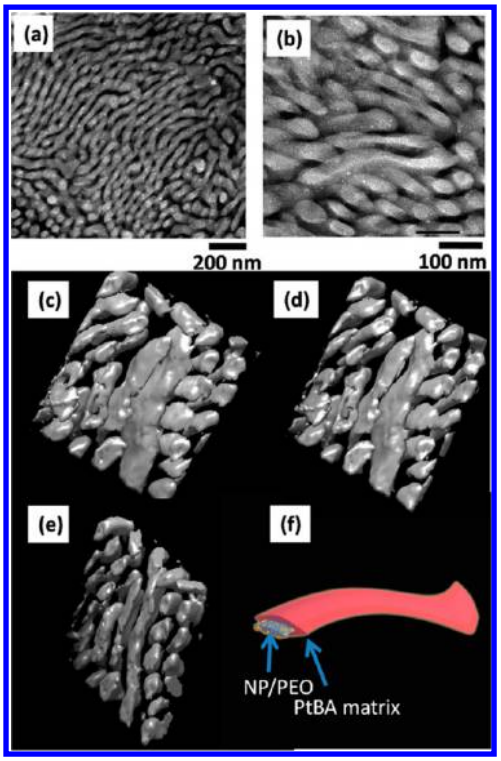

Figure 7. (a) HAADF-STEM micrograph of a blend of BBCP-**G** (f_{PEO} = 0.278) with gold NPs at f_{NP} = 0.215 ($f_{NP/PEO}$ = 0.433). (b) HAADF-STEM micrograph at a higher magnfication. (c, d, e) 3D reconstruction at different viewing angles generated by HAADF-STEM tomography. (f) Illustration of highly deformed cylinders of NP arrays with P*t*BA as the matrix.

composition the lamellar morphology leads to a more efficient molecular packing.

Figure 5b shows the SAXS profiles of a series of samples based on BBCP-**H** (f_{PEO} = 0.474). Despite the large difference in side chain lengths, well-ordered lamellar morphologies were developed in both the neat polymer and composite samples as indicated by SAXS (Figure 5b), indicating that the morphology of BBCP or BBCP/NP composites is not only dependent on the difference in side chains but also determined by volume fraction. The lamellar structure of NP arrays changed from relatively symmetric into asymmetric with the increased f_{NP} at 0.291 ($f_{NP/PEO}$ = 0.627 in Figure 5b). The well-ordered lamellar morphologies were further confirmed by TEM of the microtomed samples. As shown in Figure 8, symmetric lamellar structures were observed in the nanocomposites with moderate NP loadings ($f_{NP/PEO}$ = 0.498 and 0.555), while an asymmetric lamellar structure was obtained in the highly filled nanocomposites (see TEM 0.679 in Figure 8) consistent with the SAXS results (Figure 5b).

CONCLUSIONS

Small NP (~2 nm) assembly in P*t*BA-*b*-PEO BBCPs via hydrogen bonding was systematically investigated by taking into consideration both volume fraction of all components and side chain symmetry of the BBCPs (see Figure 9). The total volume fraction ($f_{NP/PEO}$) of the NP incorporated PEO domain strongly influenced the final morphologies of the resulting hybrids. For nanocomposites based on symmetric BBCPs (P*t*BA$_{8.2K}$-*b*-PEO$_{5.0K}$), lamellar morphologies were obtained at an exceptionally small $f_{NP/PEO}$ of only 0.248 possibly due to the

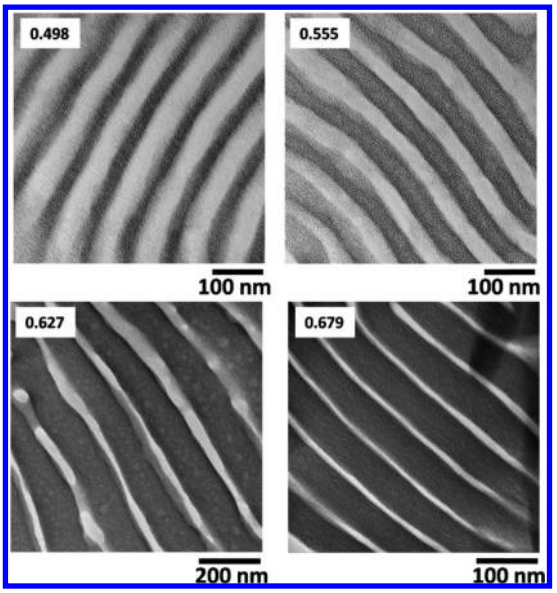

Figure 8. Cross-sectional TEM micrographs of blends of BBCP-**H** (f_{PEO} = 0.474) with gold NPs at different volume fractions. The inset numbers refer to volume fractions ($f_{NP/PEO}$) of the NP incorporated PEO domain. No staining was applied on composite samples.

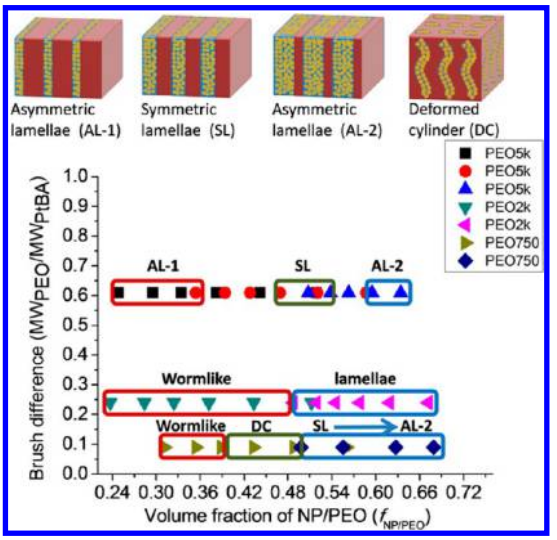

Figure 9. Summary of the morphologies of BBCP/NP composites obtained through the variation of volume fraction and side chain symmety of the BBCPs.

rigid molecular backbone of the BBCPs which favors the flat domain interface of the lamellar morphology. Symmetric and asymmetric lamellar NP arrays are available simply by changing volume fraction ($f_{NP/PEO}$). For nanocomposites based on asymmetric BBCPs (P*t*BA$_{8.2K}$-*b*-PEO$_{2.0K}$ or P*t*BA$_{8.2K}$-*b*-PEO$_{0.75K}$), various wormlike and cylindrical morphologies were developed at $f_{NP/PEO}$ approximately less than 0.488. A cylindrical morphology with highly deformed cylinders was observed in nanocomposites based on BBCPs with short PEO side chains (P*t*BA$_{8.2K}$-*b*-PEO$_{0.75K}$), which may impart additional flexibility to the PEO block reducing steric repulsion associated with the packing of longer side chains. Despite the highly asymmetric BBCPs in side chain, well-ordered lamellar structures were obtained by increasing the $f_{NP/PEO}$ to up to approximately 0.498. This work provides new insight into the phase behavior of BBCP/NP nanocomposites and indicates

DOI: 10.1021/acs.macromol.6b01602
Macromolecules XXXX, XXX, XXX−XXX

that the morphology of NP arrays can be easily tuned through the variations of both volume fraction and side chain symmetry of BBCPs. The development of strategies for control over the microstructure of NP arrays assembled in BBCP templates is essential for future functional materials design.

■ ASSOCIATED CONTENT

Supporting Information

The Supporting Information is available free of charge on the ACS Publications website at DOI: 10.1021/acs.macromol.6b01602.

Representative ^{1}H NMR spectrum and GPC light scattering traces of the brush block copolymers; reflection spectrum of composite samples; form factor fitting of SAXS (PDF)

■ AUTHOR INFORMATION

Corresponding Author

*E-mail watkins@polysci.umass.edu; Tel 413-545-2569; Fax 413-545-0082 (J.J.W.).

Notes

The authors declare no competing financial interest.

■ ACKNOWLEDGMENTS

The authors acknowledge the use of the Xeuss USAXS equipment at the Changchun Institute of Applied Chemistry (CIAC) in China. We thank Prof. Yongfeng Men of CIAC for their assistance with the USAXS experiments. We thank Maozhu Mao of University of Massachusetts Amherst for his contribution on the artwork illustration of the deformed NP cylinders. This work was supported by the NSF Center for Hierarchical Manufacturing at the University of Massachusetts (CMMI-1025020).

■ REFERENCES

(1) Talapin, D. V.; Lee, J.-S.; Kovalenko, M. V.; Shevchenko, E. V. Prospects of Colloidal Nanocrystals for Electronic and Optoelectronic Applications. *Chem. Rev.* **2010**, *110*, 389−458.

(2) Orilall, M. C.; Wiesner, U. Block Copolymer Based Composition and Morphology Control in Nanostructured Hybrid Materials for Energy Conversion and Storage: Solar Cells, Batteries, and Fuel Cells. *Chem. Soc. Rev.* **2011**, *40*, 520−535.

(3) Huynh, W. U.; Dittmer, J. J.; Alivisatos, A. P. Hybrid Nanorod-Polymer Solar Cells. *Science* **2002**, *295*, 2425−2427.

(4) Lopes, W. A.; Jaeger, H. M. Hierarchical Self-Assembly of Metal Nanostructures on Diblock Copolymer Scaffolds. *Nature* **2001**, *414*, 735−738.

(5) Briseno, A. L.; Yang, P. Optoelectronics: Combining Chemical Worlds. *Nat. Mater.* **2009**, *8*, 7−8.

(6) De Rosa, C.; Auriemma, F.; Di Girolamo, R.; Pepe, G. P.; Napolitano, T.; Scaldaferri, R. Enabling Strategies in Organic Electronics Using Ordered Block Copolymer Nanostructures. *Adv. Mater.* **2010**, *22*, 5414−5419.

(7) Wei, Q. S.; Lin, Y.; Anderson, E. R.; Briseno, A. L.; Gido, S. P.; Watkins, J. J. Additive-Driven Assembly of Block Copolymer−Nanoparticle Hybrid Materials for Solution Processable Floating Gate Memory. *ACS Nano* **2012**, *6*, 1188−1194.

(8) Bockstaller, M. R.; Mickiewicz, R. A.; Thomas, E. L. Block Copolymer Nanocomposites: Perspectives for Tailored Functional Materials. *Adv. Mater.* **2005**, *17*, 1331−1349.

(9) Kao, J.; Thorkelsson, K.; Bai, P.; Rancatore, B. J.; Xu, T. Toward Functional Nanocomposites: Taking the Best of Nanoparticles, Polymers, and Small Molecules. *Chem. Soc. Rev.* **2013**, *42*, 2654−2678.

(10) Sarkar, B.; Alexandridis, P. Block Copolymer−Nanoparticle Composites: Structure, Functional Properties, and Processing. *Prog. Polym. Sci.* **2015**, *40*, 33−62.

(11) Bockstaller, M. R.; Lapetnikov, Y.; Margel, S.; Thomas, E. L. Size-Selective Organization of Enthalpic Compatibilized Nanocrystals in Ternary Block Copolymer/Particle Mixtures. *J. Am. Chem. Soc.* **2003**, *125*, 5276−5277.

(12) Chiu, J. J.; Kim, B. J.; Kramer, E. J.; Pine, D. J. Control of Nanoparticle Location in Block Copolymers. *J. Am. Chem. Soc.* **2005**, *127*, 5036−5037.

(13) Lin, Y.; Böker, A.; He, J. B.; Sill, K.; Xiang, H. Q.; Abetz, C.; Li, X. F.; Wang, J.; Emrick, T.; Long, S.; Wang, Q.; Balazs, A.; Russell, T. P. Self-Directed Self-Assembly of Nanoparticle/ Copolymer Mixtures. *Nature* **2005**, *434*, 55−59.

(14) Balazs, A. C.; Emrick, T.; Russell, T. P. Nanoparticle Polymer Composites: Where Two Small Worlds Meet. *Science* **2006**, *314*, 1107−1110.

(15) Kim, B. J.; Chiu, J. J.; Yi, G. R.; Pine, D. J.; Kramer, E. J. Nanoparticle-Induced Phase Transitions in Diblock-Copolymer Films. *Adv. Mater.* **2005**, *17*, 2618−2622.

(16) Kim, B. J.; Bang, J.; Hawker, C. J.; Chiu, J. J.; Pine, D. J.; Jang, S. G.; Yang, S. M.; Kramer, E. J. Creating Surfactant Nanoparticles for Block Copolymer Composites Through Surface Chemistry. *Langmuir* **2007**, *23*, 12693−12703.

(17) Pang, X.; He, Y.; Jiang, B.; Iocozzia, J.; Zhao, L.; Guo, H.; Liu, J.; Akinc, M.; Bowler, N.; Tan, X.; Lin, Z. Block Copolymer/Ferroelectric Nanoparticle Nanocomposites. *Nanoscale* **2013**, *5*, 8695−8702.

(18) Lin, Y.; Daga, V. K.; Anderson, E. R.; Gido, S. P.; Watkins, J. J. Nanoparticle-Driven Assembly of Block Copolymers: A Simple Route to Ordered Hybrid Materials. *J. Am. Chem. Soc.* **2011**, *133*, 6513−6516.

(19) Yao, L.; Lin, Y.; Watkins, J. J. Ultra High Loading of Nanoparticles into Ordered Block Copolymer Composites. *Macromolecules* **2014**, *47*, 1844−1849.

(20) Jang, S. G.; Kramer, E. J.; Hawker, C. J. Controlled Supramolecular Assembly of Micelle-Like Gold Nanoparticles in PS-b-P2VP Biblock Copolymers *via* Hydrogen Bonding. *J. Am. Chem. Soc.* **2011**, *133*, 16986−16996.

(21) Jang, S. G.; Khan, A.; Hawker, C. J.; Kramer, E. J. Morphology Evolution of PS-b-P2VP Diblock Copolymers *via* Supramolecular Assembly of Hydroxylated Gold Nanoparticles. *Macromolecules* **2012**, *45*, 1553−1561.

(22) Warren, S. C.; Messina, L. C.; Slaughter, L. S.; Kamperman, M.; Zhou, Q.; Gruner, S. M.; DiSalvo, F. J.; Wiesner, U. Ordered Mesoporous Materials from Metal Nanoparticle-Block Copolymer Self-Assembly. *Science* **2008**, *320*, 1748−1752.

(23) Zhao, Y.; Thorkelsson, K.; Mastroianni, A. J.; Schilling, T.; Luther, J. M.; Rancatore, B. J.; Matsunaga, K.; Jinnai, H.; Wu, Y.; Poulsen, D.; Fréchet, J. M. J.; Alivisatos, A. P.; Xu, T. Small-Molecule-Directed Nanoparticle Assembly towards Stimuli-Responsive Nanocomposites. *Nat. Mater.* **2009**, *8*, 979−985.

(24) Kao, J.; Xu, T. Nanoparticle Assemblies in Supramolecular Nanocomposite Thin Films: Concentration Dependence. *J. Am. Chem. Soc.* **2015**, *137*, 6356−6365.

(25) Verduzco, R.; Li, X.; Pesek, S. L.; Stein, G. E. Structure, Function, Self-Assembly, and Applications of Bottlebrush Copolymers. *Chem. Soc. Rev.* **2015**, *44*, 2405.

(26) Runge, M. B.; Bowden, N. B. Synthesis of High Molecular Weight Comb Block Copolymers and Their Assembly into Ordered Morphologies in the Solid State. *J. Am. Chem. Soc.* **2007**, *129*, 10551−10560.

(27) Rzayev, J. Synthesis of Polystyrene−Polylactide Bottlebrush Block Copolymers and Their Melt Self-Assembly into Large Domain Nanostructures. *Macromolecules* **2009**, *42*, 2135−2141.

(28) Bolton, J.; Bailey, T. S.; Rzayev, J. Large Pore Size Nanoporous Materials from the Self-Assembly of Asymmetric Bottlebrush Block Copolymers. *Nano Lett.* **2011**, *11*, 998−1001.

(29) Rzayev, J. Molecular Bottlebrushes: New Opportunities in Nanomaterials Fabrication. *ACS Macro Lett.* **2012**, *1*, 1146−1149.

DOI: 10.1021/acs.macromol.6b01602
Macromolecules XXXX, XXX, XXX−XXX

(30) Fenyves, R.; Schmutz, M.; Horner, I. J.; Bright, F. V.; Rzayev, J. Aqueous Self-Assembly of Giant Bottlebrush Block Copolymer Surfactants as Shape-Tunable Building Blocks. *J. Am. Chem. Soc.* **2014**, *136*, 7762−7770.
(31) Xia, Y.; Olsen, B. D.; Kornfield, J. A.; Grubbs, R. H. Efficient Synthesis of Narrowly Dispersed Brush Copolymers and Study of Their Assemblies: The Importance of Side Chain Arrangement. *J. Am. Chem. Soc.* **2009**, *131*, 18525−18532.
(32) Sveinbjörnssona, B. R.; Weitekamp, R. A.; Miyake, G. M.; Xia, Y.; Atwater, H. A.; Grubbs, R. H. Rapid Self-Assembly of Brush Block Copolymers to Photonic Crystals. *Proc. Natl. Acad. Sci. U. S. A.* **2012**, *109*, 14332−14336.
(33) Macfarlane, R. J.; Kim, B.; Lee, B.; Weitekamp, R. A.; Bates, C. M.; Lee, S. F.; Chang, A. B.; Delaney, K. T.; Fredrickson, G. H.; Atwater, H. A.; Grubbs, R. H. Improving Brush Polymer Infrared One-Dimensional Photonic Crystals *via* Linear Polymer Additives. *J. Am. Chem. Soc.* **2014**, *136*, 17374−17377.
(34) Choo, Y.; Mahajan, L. H.; Gopinadhan, M.; Ndaya, D.; Deshmukh, P.; Kasi, R. M.; Osuji, C. O. Phase Behavior of Polylactide-Based Liquid Crystalline Brushlike Block Copolymers. *Macromolecules* **2015**, *48*, 8315.
(35) Song, D.-P.; Lin, Y.; Gai, Y.; Colella, N. S.; Li, C.; Liu, X.-H.; Gido, S.; Watkins, J. J. Controlled Supramolecular Self-Assembly of Large Nanoparticles in Amphiphilic Brush Block Copolymers. *J. Am. Chem. Soc.* **2015**, *137*, 3771−3774.
(36) Song, D.-P.; Li, C.; Colella, N. S.; Lu, X.; Lee, J.-H.; Watkins, J. J. Metallodielectric Photonic Crystals from the Self-Assembly of Brush Block Copolymers and Gold Nanoparticles. *Adv. Opt. Mater.* **2015**, *3*, 1169−1175.
(37) Song, D.-P.; Li, C.; Colella, N. S.; Xie, W.; Li, S.; Lu, X.; Gido, S.; Lee, J.-H.; Watkins, J. J. Large Volume Self-Organization of Polymer/Nanoparticle Hybrids with Millimeter Scale Grain Sizes Using Brush Block Copolymers. *J. Am. Chem. Soc.* **2015**, *137*, 12510−12513.
(38) Song, D.-P.; Li, C.; Li, W.; Watkins, J. J. Block Copolymer Nanocomposites with High Refractive Index Contrast for One-Step Photonics. *ACS Nano* **2016**, *10*, 1216−1223.
(39) Gu, W.; Huh, J.; Hong, S. W.; Sveinbjornsson, B. R.; Park, C.; Grubbs, R. H.; Russell, T. P. Self-Assembly of Symmetric Brush Diblock Copolymers. *ACS Nano* **2013**, *7*, 2551−2558.
(40) Chremos, A.; Theodorakis, P. E. Morphologies of Bottle-Brush Block Copolymers. *ACS Macro Lett.* **2014**, *3*, 1096−1100.
(41) Dalsin, S. J.; Rions-Maehren, T. G.; Beam, M. D.; Bates, F. S.; Hillmyer, M. A.; Matsen, M. W. Bottlebrush Block Polymers: Quantitative Theory and Experiments. *ACS Nano* **2015**, *9*, 12233−12245.

DOI: 10.1021/acs.macromol.6b01602
Macromolecules XXXX, XXX, XXX−XXX